

n-ZnO/p-Cu₂O Heterojunction Electrode: Characterization and Evaluation of Their Photoelectrochemical Properties

Edson Archela¹, Luan Pereira de Camargo², Marcelo Rodrigues da Silva Pelissari², Luiz Henrique Dall'Antonia^{1,*}

¹ Departamento de Química, Universidade Estadual de Londrina, 86057-970 Londrina – PR, Brazil.

² UNESP - Universidade Estadual Paulista, Faculdade de Engenharia, Colégio Técnico Industrial, 17033-260, Bauru, SP, Brazil.

*E-mail: luizh@uel.br

Received: 18 July 2018 / Accepted: 10 January 2019 / Published: 10 March 2019

In this work an easy way to prepared heterojunction electrodes based on ZnO and Cu₂O were developed. The electrodes were synthesized by a simple electrodeposition method. The photoelectrodes obtained were not submitted to a high temperature treatment. The electrodeposited films prevent the recombination of photogenerated charge carriers and thus allow the continuous formation of electrons and holes on photoelectrocatalytic reactions. Moreover, the films electrodeposited were characterized by X-ray diffraction, Raman spectroscopy, scanning electronic microscopy and UV-Vis. The photoelectrochemical activity was evaluated under visible light irradiation. The Cu₂O addition at the photoelectrodes were efficient to improve the properties of pure ZnO and also promote superior photoelectrochemical and photoelectrocatalytic responses for methylene blue discoloration.

Keywords: Thin film, photoelectrodes, hexagonal phase, methylene blue.

1. INTRODUCTION

Photocatalytic and photoelectrocatalytic devices have aroused great interest in recent years due to the fact of using, in their configuration, solar energy for the hydrogen gas production, degradation of organic pollutants in aqueous medium and generation of clean electric energy [1-4]. About the configuration and architecture of photoelectrocatalytic system, some studies are concentrated in the use of n-type electrodes, called photoanodes, such as TiO₂ [5], ZnO [6], CdS [7] and BiVO₄ [8, 9]. In another hand, p-type electrodes, called photocathodes, are still little explored. However, some previously published works report the use of them, such as NiO [10], Cu₂O [4, 11] and CaFe₂O₄ [12].

Zinc oxide (ZnO) is classified as a n-type semiconductor material with a wide band gap energy of 3.37 eV [13, 14]. This oxide material has been widely used in photocatalysis and photoelectrocatalysis application due to its high chemistry stability in aqueous medium, high electrical conductivity, low cost of production, non-toxic, and can be obtained in nano-size domain in different particle shape [6, 13, 14]. For example, *Lucilha and co-workers* [6] synthesized ZnO and Ag-ZnO nano-crystal for heterogeneous photocatalysis application. The obtained results showed that Ag-ZnO more than doubled the decolorization rate constant with respect to ZnO, attributed to the increase of available surface area, as well as the recombination decrease of the photogenerated charge carriers, by removal of electrons by silver, generating hydroxyl radical.

ZnO oxide semiconductor material can be obtained by numerous different techniques, such as chemical vapor deposition [15], thermal evaporation [16], hydrothermal processing [17], sol-gel [18] metal-organic chemical vapor deposition [19], chemical spray pyrolysis [20], electrodeposition process [14, 21], among others. Electrodeposition process is technologically attractive, being fast, simple, low-cost technique and control over film thickness. Besides, this process can produce nanostructured thin film materials, which is a very important parameter for the photoelectrocatalysis application [14].

In another hand, the cuprous oxide (Cu_2O) is known a p-type semiconductor material due the intrinsic copper atoms vacancies in the Cu_2O lattice [4, 22, 23]. This oxide material presents direct band gap energy of 2 eV and theoretical visible light conversion efficiency in electric energy of about 20% [24]. In the Cu_2O semiconductor, the valence and conduction bands positions are close to the redox potential of water. This factor makes the Cu_2O a viable candidate for the use as electrode material in direct hydrogen production by water photolysis driven visible light irradiation [25, 26]. In order to obtain nanostructured Cu_2O thin film format, various physical and chemical techniques have been used, such as, thermal oxidation [27], chemical vapor deposition [28], plasma evaporation [29], reactive sputtering [30], electrodeposition [4, 11, 23, 23], among others.

The effect of photogenerated charge carriers separation with high efficiency is the key to the high quantum efficiency of the photoanode and photocathodes electrodes, leading to an improved photoelectrochemical performance of photoelectrocatalytic system [9]. The combination of photoactive semiconductor materials as heterojunctions seems to be an interesting approach, where a well-designed interface may lead to photoinduced charge separation and the suppression of electron-hole recombination [31]. In this context, n-ZnO and p- Cu_2O semiconductor emerge as important materials to construction of p-n heterojunction electrode. Previously published papers have dealt with the use of Cu_2O and ZnO as p-n heterojunctions electrodes in photoelectrocatalysis device. For example, *Bial and co-workers* [32] synthesized a novel three dimensional (3D) ZnO/ Cu_2O nanowire photocathode material by chemical oxidation and hydrothermal growth methods. Compared with the isolated Cu_2O NWs, the 3D ZnO/ Cu_2O NWs showed a highly efficient photoelectrocatalytic performance, with a larger photocurrent (-4.55 mA cm^{-2}) and better stability under continuous illumination. More recently, *Lahmar and co-workers* [33] synthesized p- Cu_2O /n-ZnO heterojunction directly on fluorine-doped tin oxide (FTO) substrate by two electrodeposition step in aqueous solution. The p- Cu_2O /n-ZnO heterojunction show long electron lifetime and high electron-hole separation efficiency according to the electrochemical impedance spectroscopy (EIS) measurements and photocurrent response.

This paper deals with the synthesis, characterization and potential application of n-ZnO/p-Cu₂O heterojunction material in photoelectrochemical system. To the construction and architecture of device, we used the simple, low-cost and efficiently electrodeposition process. The material in the thin film format were electrodeposited on conductor indium-doped tin oxide (ITO) electrode and characterized physically by XRD, Raman, SEM and UV-Vis. The photoelectrochemical measurements were carried out by cyclic voltammetry (CV) and chronoamperometry techniques in the 0.1 mol L⁻¹ phosphate-buffered saline (PBS) solution.

2. EXPERIMENTAL

2.1. Synthesis of ZnO, Cu₂O and n-ZnO/p-Cu₂O thin film electrodes

The ZnO and Cu₂O thin films were obtained by electrodeposition process on indium-doped tin oxide (ITO) electrode, adapted from widely published procedures [4, 11, 14, 22, 27, 33, 34]. Firstly, ITO substrates were washed with sodium hydroxide (NaOH, 1 mol L⁻¹) and hydrogen peroxide (H₂O₂, 30 %) solutions. After, the substrates were rinsed several times in acetone and deionized water, and dried at room temperature. The ZnO thin film was obtained by electrodeposition process in 5 mmol L⁻¹ of zinc nitrate hexahydrate (Synth, 99.4%) and 0.1 mol L⁻¹ of potassium nitrate (Synth, 99.4%). The ITO substrate was immersed in this solution and a fixed potential of -1.15 V was applied, at 70 °C for 20 min. The Cu₂O thin film was obtained by electrodeposition process in 1 mmol L⁻¹ of copper sulphate hexahydrate (Synth, 99.5%) and 0.1 mol L⁻¹ of citric acid (Synth, 99.5%). The pH this solution was adjusted to 11 by dropwise addition of 0.1 mol L⁻¹ of sodium hydroxide. The ITO substrate was immersed in this solution and a fixed potential of -0.4 V was applied, at 60 °C for 20 min. Then, the obtained film was dried in muffle oven for 1 hour at 100 °C. The n-ZnO/p-Cu₂O heterojunction electrode was obtained by electrodeposition of ZnO thin film over ITO substrate, followed by electrodeposition of Cu₂O over ZnO thin film surface. Both the obtained films, in the isolated and heterojunction forms, were dried in muffle oven for 1 hour at 100 °C.

2.2. Physical Characterization

X-ray diffraction (XRD) measurements were carried out using a PANalytical diffractometer, model X'Pert PRO MPD, with the CuK α (1.5418 Å) radiation, coupled to a nickel filter, in order to reduce the unfavorable CuK β radiation. The applied tension was 40 kV and the current was 30 mA. The scanning range was from 10° to 80°, with regular step of 0.05° s⁻¹. Scanning electron microscopy (SEM) images were obtained in a Quanta 200-FEI microscope with 30 kV of applied voltage. Raman scattering data were obtained by Renishaw 3000 spectrometer, with excitation at 523 nm. The scanning system works with accumulation of 256 scans and 2 cm⁻¹ spectral resolution. The optical absorption spectra were determined with the help of Shimadzu UV-2600 PC equipment within the range 200–800 nm.

2.3. Photoelectrochemical measurements

Conventional electrochemical cell with three electrodes were used for the electrochemical and photoelectrochemical experiments, where an Ag/AgCl (3 mol L⁻¹ KCl) is the reference electrode, a platinum wire (10 cm in length and 0.5 mm in diameter) is the counter electrode, and the ZnO, Cu₂O and ZnO/Cu₂O thin films, deposited on ITO conductor substrate are the work electrodes (the geometrical electrode area in contact with the solution is set to 1 cm²). The light irradiation in the electrochemical system is done through a Philips dichroic lamp with a power of 50 W at an applied voltage of 12 V. This light source presents wide spectra, with emission from $\lambda \geq 400$ nm. It must be mentioned that illumination was done in the front part of the p-n junction electrode. The photoelectrochemical characterization procedures are carried out by cyclic voltammetry and chronoamperometry techniques, through a potentiostat/galvanostat Autolab 84057, version 4.9, using 0.1 mol L⁻¹ phosphate-buffered saline (PBS) solution as electrolyte support.

For the methylene blue (MB) degradation tests, was used a solution contend 16 $\mu\text{mol L}^{-1}$ of methylene blue and 0.1 mol L⁻¹ of phosphate-buffered saline (PBS) solution as electrolyte support. The MB degradation evaluation was carried out by chronoamperometry technique, with controlled potential of +0.2 V during different degradation times. After degradation, aliquots were withdrawn at different times (0 – 90 min), and put inside quartz cuvette to verify the relative (percentage) amount of MB that had vanished. The adopted parameter was the decreasing of the MB optical absorption band, taken at approximately 665 nm. These spectra were taken just after the chronoamperometry measurements by Ocean Optics USV-4000 spectrophotometer with 5 scans and integration time of 20 Ms.

3. RESULTS AND DISCUSSION

3.1. Physical Characterization

The X-ray results obtained from ZnO, Cu₂O and ZnO/Cu₂O films, are shown in Fig. 1. In all diffractograms it is possible to observe the diffraction peaks of the ITO substrate. The diffracted peaks in Cu₂O at about $2\theta = 29.6^\circ$, 36.5° , 42.3° and 73.6° , associated with the crystallographic planes (110), (111), (200) and (311), are due the cubic system with spatial group Pn-3m (224) and lattice parameter $a = 4.258 \text{ \AA}$, as obtained by comparison with the crystallographic pattern (PCPDFWIN software, version 2.4, JCODS-ICDD, card 77-0199). The diffracted peaks in ZnO at about $2\theta = 31.8^\circ$, 34.3° , 36.2° , 47.4° , 56.5° , 62.8° and 67.8° , associated with the crystallographic planes (100), (002), (101), (102), (110), (103) and (112), are due the hexagonal system that belongs to spatial group P63mc (186), with lattice parameters $a = b = 3.2498 \text{ \AA}$, and $c = 5.2066 \text{ \AA}$ (card 36-1451 of the same mentioned software).

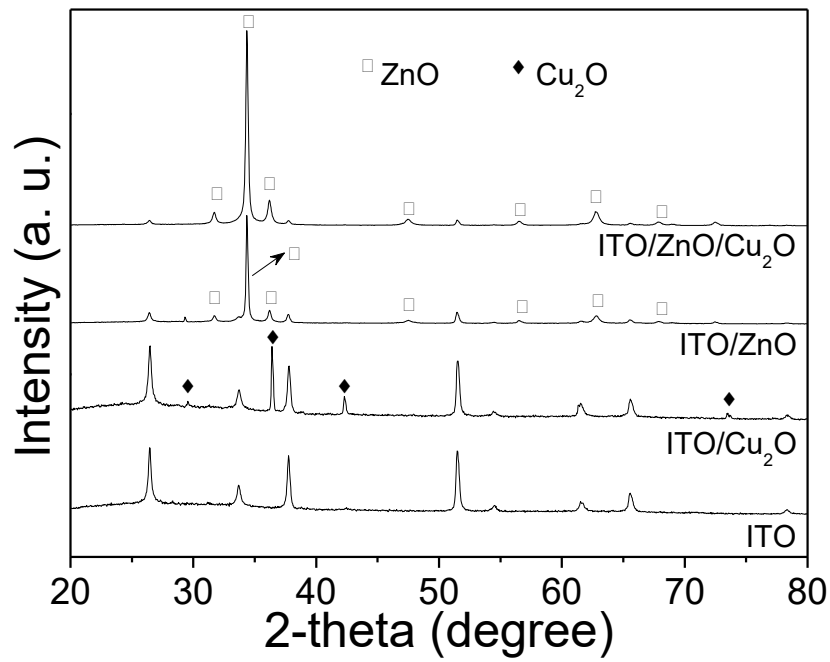


Figure 1. X-ray diffractogram of ZnO, Cu₂O and ZnO/Cu₂O thin films electrodeposited on ITO substrate.

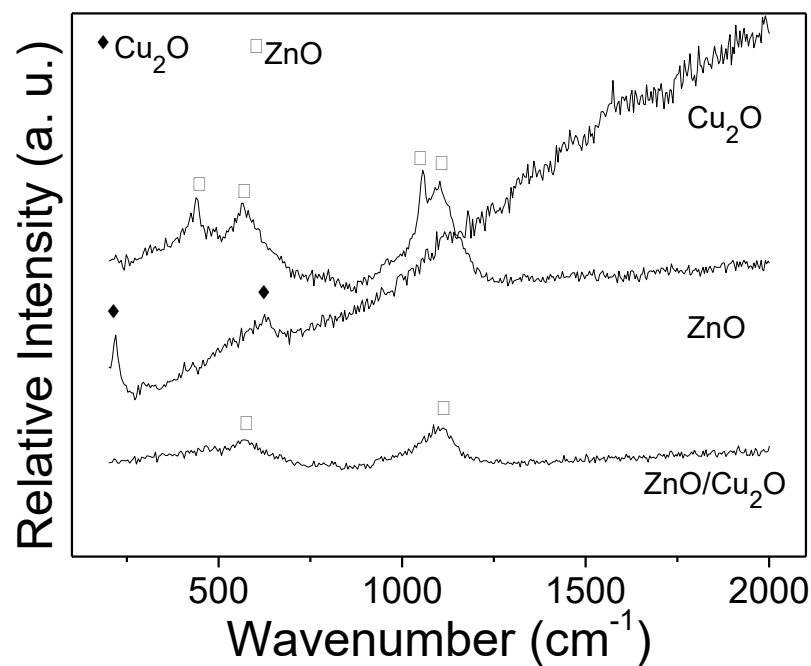


Figure 2. Raman spectra of ZnO, Cu₂O and ZnO/Cu₂O thin films electrodeposited on ITO substrate.

The obtained diffraction patterns are in good agreement with previously published reports, with samples either in the nanocrystalline thin film form [13, 14, 22, 23, 27, 34], obtained by electrodeposition

process. In the diffractograms of ZnO/Cu₂O it is possible to observe only the diffracted peaks of hexagonal structure of ZnO photoelectrode. In this case, it is possible that the high intensity of diffracted peaks of ZnO hexagonal structure make it difficult to visualize of the cuprous oxide peaks. In addition, it is possible too that on the ZnO/Cu₂O surface has a smaller amount of Cu₂O phase, when compared whit ZnO phase.

The Raman spectra of ZnO, Cu₂O and ZnO/Cu₂O films are shown in Fig. 2. In Cu₂O thin film structure, the strong peak at 212 cm⁻¹ and the weak peak at 628 cm⁻¹ originated from the Raman-allowed mode of the Cu₂O crystals. This result is in good agreement with some published reports [35-37]. Concerning the Raman spectra of ZnO photoelectrode, the peaks at about 439 cm⁻¹ and 563 cm⁻¹ are associated with first-order Raman scattering from the ZnO vibrational modes [38], and the peak at 439 cm⁻¹ is typical of wurtzite structure. Besides, others two peaks are visualized on ZnO Raman spectra, the peaks at about 1059 cm⁻¹ and 1104 cm⁻¹ that are associated with 2LO vibrational mode of ZnO crystal [39]. In the Raman spectra of ZnO/Cu₂O heterojunction, when Cu₂O is the top layer, are visualized tow peaks associated with ZnO vibrational modes, 563 cm⁻¹ and 1104 cm⁻¹. In this case, the peaks associated with de Cu₂O crystal not appears. This results obtained by Raman spectroscopy are in good agreement with the XRD results discussed above. In both techniques, it's not possible to check the Cu₂O phase in the ZnO/Cu₂O heterojunction configuration electrode.

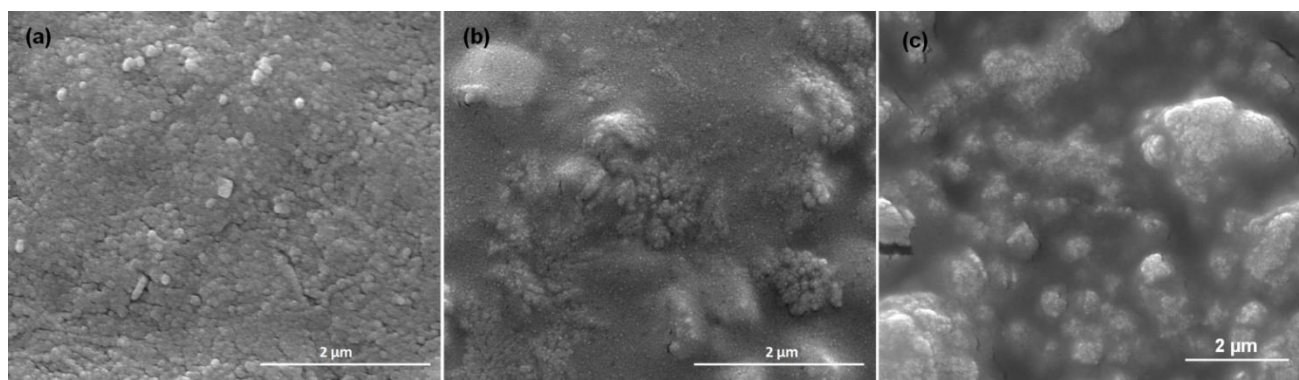


Figure 3. SEM surface images with different magnifications of (a) ZnO, (b) Cu₂O and (c) ZnO/Cu₂O thin films.

SEM topographic images of ZnO, Cu₂O and ZnO/Cu₂O films electrodeposited on ITO conductor substrate can be seen in Fig. 3. In the ZnO photoelectrode (Fig. 3a) the surface image is quite homogeneous, being formed of round-shaped particles homogeneously distributed throughout the investigated area. In the other hand, the surface image of the Cu₂O photoelectrode (Fig. 3b) is not homogeneous, with some areas formed by aggregates of particles with spherical shape. Figure 3c corresponds to ZnO/Cu₂O, when Cu₂O is the top layer. The image shown that in the heterojunction thin film the surface is similar to the Cu₂O surface (Fig. 3b), a non-homogeneous surface with some deep regions formed by channels surrounded by aggregate particles, which may leading to a high roughness surface, implying in a higher surface area. This surface behavior may be very interesting for electrochemical system which means greater efficiency.

Diffuse reflectance UV-Vis spectra for the all samples are shown in Fig. 4a. The fundamental absorption edge for the ZnO thin film starts at about 290 nm and then two absorption bands appear, one at about 337 nm and other at 383nm, which are typical behavior of thin film material [14]. Besides, from 600 nm, the transmittance of ZnO thin film is lower than Cu₂O and ZnO/Cu₂O heterojunction thin film. For the Cu₂O, the fundamental absorption edge starts at about 450 nm, in the visible region of electromagnetic spectrum. Another absorption band at 340 nm in this material can be associated for the absorption of ITO substrate. In relation of ZnO/Cu₂O heterojunction, two absorptions bands appear, one at about 324 nm due the ZnO contribution material and other at 406 nm due the Cu₂O contribution. In this case, the absorption band of ZnO is shifted to higher wavelength, while the absorption band of Cu₂O is shifted to lower wavelength, which is a typical behavior of heterojunction thin films electrode material [27].

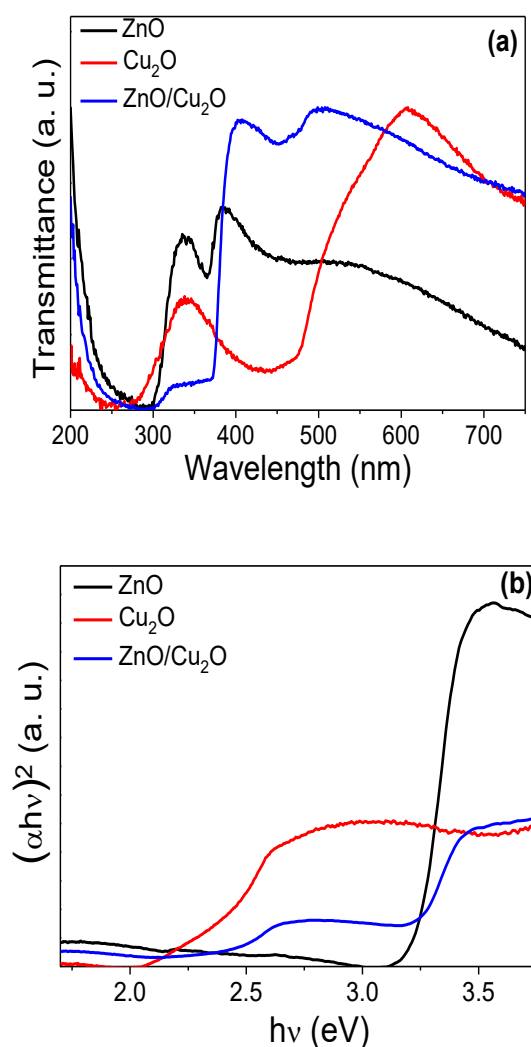
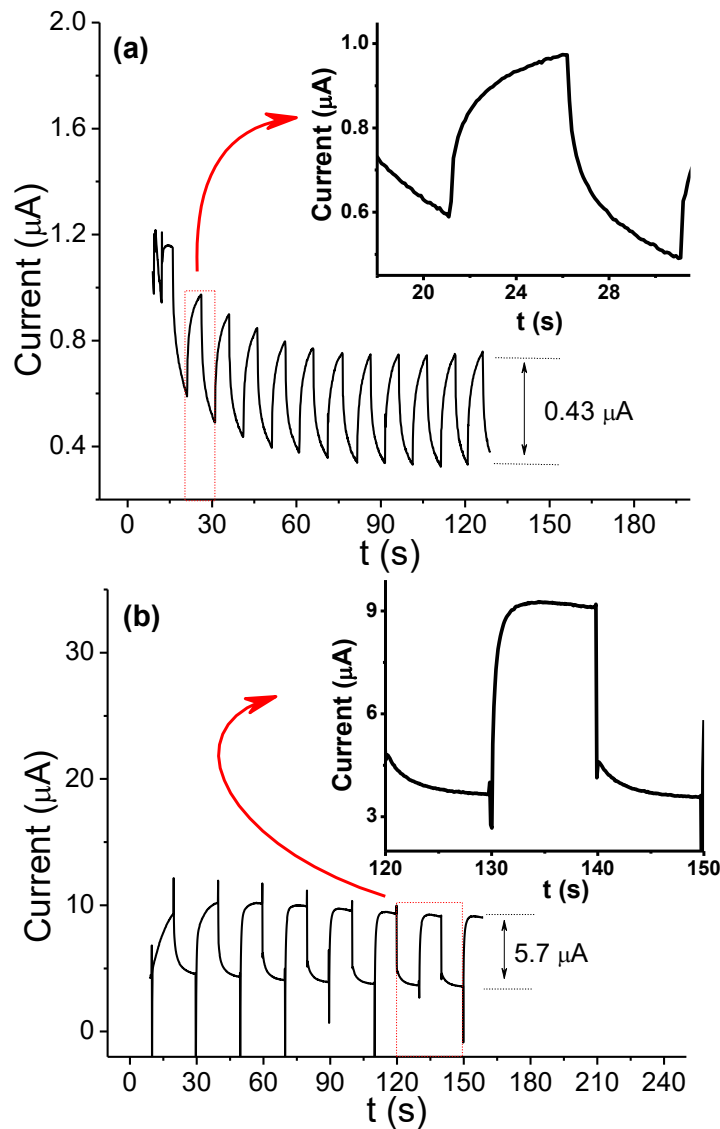


Figure 4. (a) UV-Vis optical transmittance spectra of all samples, (b) bandgap energy evaluation.

Considering direct band gap transition for the all samples [14, 27, 40, 41], the value of the band gap for this film can be evaluated using the method proposed by Wood and Tauc [42], which is in good approximation, by a plot of $(\alpha h\nu)^2$ as function of $h\nu$ plot, and taking the crossing of the slope of the linear

part with the “x” axis. The obtained results, showed in Fig. 4b, yields band gap values of about 3.3 eV, 2.3 eV and 3.2 eV for the ZnO, Cu₂O and ZnO/Cu₂O, respectively. These results are in good agreement with reported results for these materials in the form of thin films [14, 22, 27, 40, 41] obtained for electrodeposition process.

3.2. Photoelectrochemical measurements



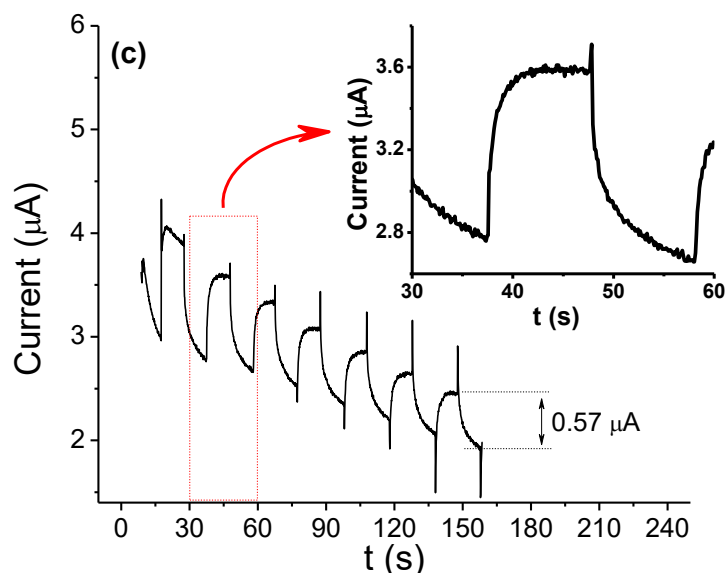


Figure 5. Photochronoamperogram of thin film electrode in $1.0 \text{ mol L}^{-1} \text{ Na}_2\text{SO}_4$ solution under chopped visible light irradiation source (dichroic lamp): (a) ZnO, (b) Cu_2O and (c) ZnO/ Cu_2O . Inset: details of stability and decay of photocurrent density. Controlled potential at $+0.2 \text{ V}$ versus Ag/AgCl.

The stability of photo-induced current was evaluated by chronoamperometry in $1.0 \text{ mol L}^{-1} \text{ Na}_2\text{SO}_4$ solution with a controlled potential at $+0.2 \text{ V}$ versus Ag/AgCl ($3 \text{ mol L}^{-1} \text{ KCl}$), under chopped visible light irradiation condition from dichroic lamp. The photochronoamperogram illustrated in Fig. 5a show the photocurrent decay profile of ZnO electrode, where is observed a decrease of 40% in the photo-induced current value during the first 80 seconds. After this time, the current value, that is obtained by the difference between the current reached under illumination (light on) and without illumination (light off) [8, 9], is equal $0.43 \mu\text{A}$. This behavior, photocurrent decay profile, is similar to the ZnO/ Cu_2O thin film electrode, Fig. 5c, where also a decrease of 40% in the photo-induced current is observed, and the current value obtained is equal $0.57 \mu\text{A}$. On the other hand, the photocurrent decay profile of Cu_2O electrode, Fig. 5b, a decrease of only 7% in the photo-induced current value is observed during all time of chronoamperogram. In this case, the current value obtained is higher than ZnO and ZnO/ Cu_2O , approximately $5.7 \mu\text{A}$. Besides, the photo-induced current acquires stability under light irradiation, as observed by inset graphic in this figure. In this case, when the light on, the photo-current increase quickly and during all time (under light on) remains stable, the same value. This behavior, photo-induced current stability, is quite similar to ZnO/ Cu_2O electrode and very different to the ZnO electrode.

The performance of these thin films electrodes was investigated by using a $10 \text{ mmol L}^{-1} \text{ MB}$ solution in $1.0 \text{ mol L}^{-1} \text{ Na}_2\text{SO}_4$ electrolyte solutions. MB degradation analysis was performed by the chronoamperometric technique at $+0.2 \text{ V}$ versus Ag/AgCl controlled potential. The results are showed in Fig. 6. Under visible light irradiation condition, a high degradation percentage of MB by all electrodes is observed. These degradation percentages are summarized in table 1.

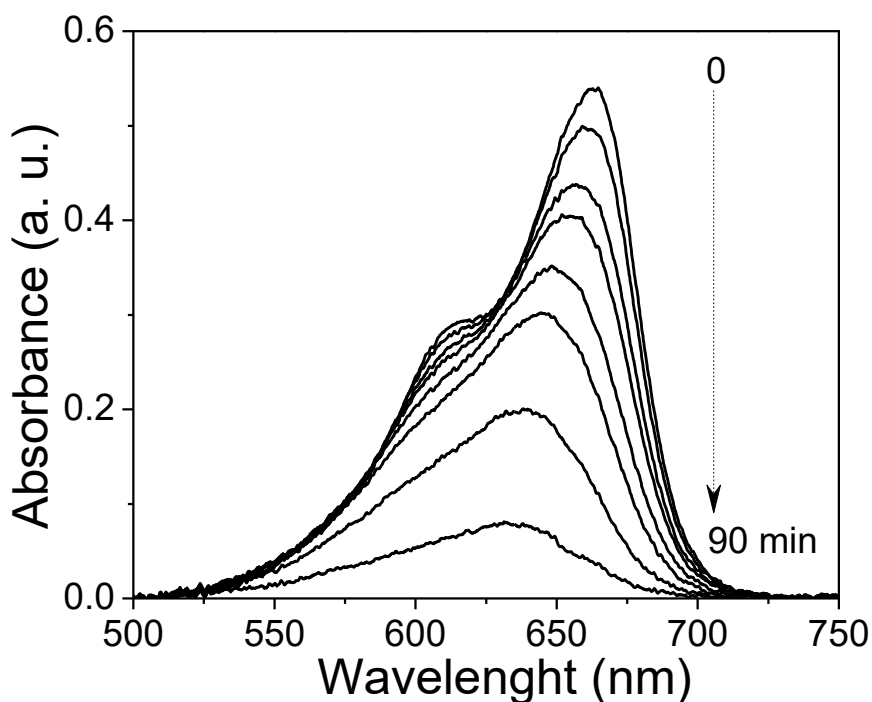


Figure 6. UV-VIS spectra of MB solution degradation in $1.0 \text{ mol L}^{-1} \text{ Na}_2\text{SO}_4$ using a ZnO/Cu₂O film under visible light irradiation and potential applied of +0.2 V versus Ag/AgCl.

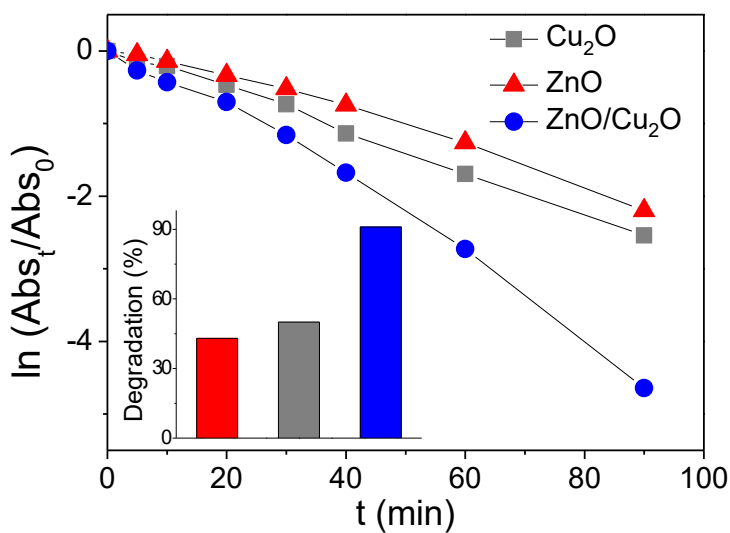


Figure 7. Decay curves of MB concentration at different degradation times in Na_2SO_4 solution under continuous visible light irradiation and potential applied of +0.2 V vs Ag/AgCl.

In this case, the photo-induced effect on the excitation of the semiconductor film, coupled with the external potential applied effect to the working electrode, provides greater system efficiency, due to generation of a higher density of charge carriers and decrease of electron-hole pairs recombination effect.

In addition, in the ZnO/Cu₂O electrode, the effect of p-n heterojunction leads to greater degradation percentage of MB molecule.

Table 1. Values of the rate constant (k_{obs}) of methylene blue discoloration ($10.0 \mu\text{mol L}^{-1}$) under visible irradiation. All measurements were carried out at room temperature applying + 0.2 V versus Ag/AgCl.

Photoelectrode	k_{obs} (10^{-3} min^{-1})	Discoloration (%)
ZnO	24.3	43
Cu ₂ O	28.6	50
ZnO/Cu ₂ O	50.1	91

Figure 7 shows the kinetics studies of MB degradation reaction. Decay profile of the curves suggests that both processes follow first-order kinetics. The rate constant of the reaction (k_{obs}) can be easily evaluated, as widely published [7, 8]. The rate constant values obtained are also summarized in Table 1. The rate constant values to ZnO, Cu₂O and ZnO/Cu₂O are 24.3, 28.6, $50.1 \times 10^{-3} \text{ min}^{-1}$, respectively. From these results, it is observed that the rate constant of MB degradation by p-n function electrodes is higher than single ZnO and Cu₂O films. Due to the visible light spectra, used for the sample excitation, a comparison with the single ZnO film sample is not adequate, because the ZnO bandgap is about 3.3 eV, in the UV range, whereas the Philips dichroic excitation source presents emission from $\lambda \geq 400 \text{ nm}$.

Due the two effect: external potential applied to the system and p-n heterojunction, in the surface of thin film materials there may be a large number of electrons/holes photogenerated charge. So, this high density of surface charge can oxidize water molecules to $\cdot\text{OH}$ type radicals that are fundamental in the MB degradation process, due to the attack to the chromophore group of the molecule [7, 8], as already mentioned.

Simple comparisons of our results with previously published results are shown below. For example, in the paper of Cui and co-workers [43], using a electrode configuration a little bit different of our work, the authors obtained 98 % of MB degradation using ZnO nanorod arrays on Cu₂O thin film. This result is higher than the result obtained in our paper. In another paper, Hajji and co-workers [44], using the electrodeposition proces, as in our paper, obtained ZnO/Cu₂O thin film electrode. The authors obtained 78 % of MB degradation with this electrode, and this result is little bit lower when compared with our result, 91 %.

4. CONCLUSION

The electrodeposition process used in this paper was quite efficient in obtaining ZnO, Cu₂O and ZnO/Cu₂O thin film semiconductor material as demonstrated by the characterization measurements carried out by XRD, Raman, SEM and UV-Vis techniques.

These thin films electrodes materials presented good photoelectrocatalytic response for the discoloration of the MB dye. However, the heterojunction photoelectrode presented a remarkable response, compared to the films alone, that can be associated with the effect of external potential applied to the system and p-n heterojunction, leads to the better preventing the fast electron-hole recombination-back process.

Overall, the results presented here allow concluding that these thin films deposited on ITO conductive electrode by fast and ease electrodeposition process stands as an important methodological tool with technological potential to be used directly in environmental preservation, specifically in the decontamination of surface water and wastewater.

CONFLICT OF INTEREST

The authors declare that they have no conflict of interest.

ACKNOWLEDGEMENTS

The authors wish to thank FUNDAÇÃO ARAUCÁRIA (15585/2010), INCT-Bio (FAPESP 14/50867-3 and CNPq 465389/2014-7) and CNPq (process 406459/2016-9) for financial support. The authors would also like to thank LARX-UEL for XRD analysis and LMEM-UEL for SEM analysis.

References

1. S.G. Kumar and K.S.R.K. Rao, *RSC Advances*, 5 (2015) 3306-3351.
2. B-X, Lei, L-L Zeng, P. Zhang, Z-F. Sun, W. Sun and X-X. Zhang, *Adv. Powder Technol.*, 25 (2014) 946–951.
3. W. Sang, G. Zhang, H. Lan, X. An and H. Liu, *Electrochim. Acta*, 231 (2017) 429–436.
4. R-M. Liang, Y-M, Chang, P-W. Wu and P. Lin, *Thin Solid Films*, 518 (2010) 7191–7195.
5. S. Pausova, S. Kment, M. Zlamal, M. Baudys, Z. Hubicka and J. Krysa, *Molecules*, (2017), 22, 775.
6. A.C. Lucilha, M.R. Silva, R.A. Ando, L.H. Dall’Antonia and K. Takashima, *Quím. Nova*, 39, (2016) 409-414.
7. A. Pareek, A. Gopalakrishnan and P.H. Borse, *J. Phys. Conf. Ser.*, 755, (2016) 1.
8. M.R. Silva, V.S.L. Neto, A.C. Lucilha, L.V.A. Scalvi and L.H. Dall’Antonia, *Ionics*, 21, (2015) 1407-1415.
9. M.R. Silva, L.V.A. Scalvi, V.S.L. Neto and L.H. Dall’Antonia, *J. Solid State Electr.*, 20, (2016) 1527-1538.
10. M.R. Silva, V.S.L. Neto, A.C. Lucilha, L.V.A. Scalvi and L.H. Dall’Antonia, *Ionics*, 21, (2015) 1407-1415.
11. L. Xu, H. Xu, S. Wu and X. Zhang, *Appl. Surf. Sci.*, 258 (2012) 4934–4938.
12. S. Ida, K. Yamada, T. Matsunaga, H. Hagiwara, Y. Matsumoto and T. Ishihara, *J. Am. Chem. Soc.*, 132 (2010) 17343–17345.

13. T. Dikici, *Ceram. Int.*, 43 (2017) 8289–8293.
14. I. Gromyko, M. Krunks, T. Dedova, A. Katerski, D. Klauson and I.O. Acik, *Appl. Surf. Sci.*, 405 (2017) 521–528.
15. G. Wang, Y. Wang, M. Yau, C. To, C. Deng and D.H. Ng, *Mater. Lett.*, 59 (2005) 3870–3875.
16. L. Feng, A. Liu, M. Liu, Y. Ma, J. Wei and B. Man, *Mater. Charact.*, 61 (2010) 128–133.
17. L. Pei, H. Zhao, W. Tan, H. Yu, Y. Chen and Q-F. Zhang, *Mater. Charact.* 60 (2009) 1063–1067.
18. M. Popa, R.A. Mereu, M. Filip, M. Gabor, T. Petrisor Jr, L. Ciontea and T. Petrisor, *Mater. Lett.*, 92 (2013) 267.
19. N. Han, P. Hu, A. Zuo, D. Zhang, Y. Tian and Y. Chen, *Sensor Actuat. B-Chem.*, 145 (2010) 114–119.
20. T. Dedova, M. Krunks, I.O. Acik, D. Klauson, O. Volobujeva and A. Mere, *Mater. Chem. Phys.* 141 (2013) 69–75.
21. C. Badre, T. Pauporté, M. Turmine and D. Lincot, *Nanotechnology*, 18 (2007) 365705.
22. I.S. Brandt, C.A. Martins, V.C. Zoldan, A.D.C. Viegas, J.H.D. Silva and A.A. Pasa, *Thin Solid Films*, 562 (2014) 144–151.
23. M.M. Moharama, E.M. Elsayed, J.C. Nino, R.M. Abou-Shahba and M.M. Rashad, *Thin Solid Films*, 616 (2016) 760–766.
24. L. Liu, Q. Xi, G. Gao, W. Yang, H. Zhou, Y. Zhao, C. Wu, L. Wang and J. Xu, *Sol. Energy Mater. Sol. Cells*, 157(2016)937–942.
25. J. Zhao, P.D. Tran, Y. Chen, S.C.J. Loo, J. Barber, and Z.J. Xu, *ACS Catal.*, 5 (2015) 4115–4120.
26. P.D. Tran, S.K. Batabyal, S.S. Pramana, J. Barber, L.H. Wong, S.C.J. Loo, *Nanoscale*, 4 (2012) 3875–3878.
27. S.S. Jeong, A. Mittiga, E. Salza, A. Masci and S. Passerini, *Electrochim. Acta*, 53 (2008) 2226–2231.
28. I. Grozdanov, *J. Mater. Lett.*, 19 (1994) 281–285.
29. V. Figueiredo, E. Elangovan, G. Goncalves, P. Barquinha, L. Pereira, N. Franco, E. Alves, R. Martins and E. Fortunato, *App. Surf. Sci.*, 254 (2008) 3949–3954.
30. H. Zhu, J. Zhang, C. Li, F. Pan, T. Wang and B. Huang, *J. Thin Solid Films*, 517 (2009) 5700–5704.
31. M.R. Silva, L.V.A. Scalvi, V.S.L. Neto, and L.H. Dall’Antonia, *J. Mater. Sci. Mater. Electron.*, 26 (2015) 7705–7714.
32. J. Bai, Y. Li, R. Wang, K. Huang, Q. Zeng, J. Li and B. Zhou, *J. Mater. Chem. A*, 3 (2015) 22996–23002.
33. H. Lahmar, F. Setifi, A. Azizi, G. Schmerber and A. Dinia, *J. Alloys Compd.*, 718 (2017) 36–45.
34. N.A. Ahmed, M. Eyraud, H. Hammache, F. Vacandio, S. Sam, N. Gabouze, P. Knauth, K. Pelzer and T. Djenizian, *Electrochim. Acta*, 94 (2014) 238–244.
35. R. Kumar, P. Rai and A. Sharma, *RSC Adv.*, 6 (2016) 3815–3822.
36. W. Yu, M. Han, K. Jiang, Z. Duan, Y. Li, Z. Hu and J. Chu, *J. Raman Spectrosc.*, 44 (2013) 142–146.
37. O. Lupan, V. Cretu, V. Postica, N. Ababii, O. Polonskyi, V. Kaidas, F. Schütt, Y.K. Mishra, E. Monaico, I. Tiginyanu, V. Sontea, T. Strunskus, F. Faupel and R. Adelung, *Sensor Actuat. B-Chem.*, 224 (2016) 434–448.
38. C. Charpentier, P. Prod’homme, I. Maurin, M. Chaigneau and P.R. Cabarrocas, *EPJ Photov.*, 2 (2011) 25002.
39. C. Roy, S. Byrne, E. McGlynn, J.P. Mosnier, E. Posada, D. O’Mahony, J.G. Lunney, M.O. Henry, B. Ryan and A.A. Cafolla, *Thin Solid Films*, 436 (2003) 273–276.
40. F. Tezcan, A. Mahmood and G. Kardas, *J. Mater. Sci. Mater. Electron.*, 29 (2018) 9547.
41. O. Messaoudi, I.B. Assaker, M. Gannouni, A. Souissi, H. Makhlof, A. Bardaoui and R. Chtourou, *App. Surf. Sci.*, 366 (2016) 383–388.
42. J. Tauc, R. Grigorovici and A. Vancu, *J. Phys. Stat. Sol.*, 15 (1966) 627–637.

43. Y. Cui, C. Wang, G. Liu, H. Yang, S. Wu, T. Wang, *Mater. Lett.*, 65 (2011) 2284–2286.
44. M.E. Hajji, A. Hallaoui, L. Bazzi, A. Benlhachemi, O. Jbara, A. Tara, B. Bakiz, *Int. J. Electrochem. Sci.*, 9 (2014) 4297–4314.

© 2019 The Authors. Published by ESG (www.electrochemsci.org). This article is an open access article distributed under the terms and conditions of the Creative Commons Attribution license (<http://creativecommons.org/licenses/by/4.0/>).